Spatiotemporal Variations in Terrestrial Water Storage and Its Controlling Factors in the Eastern Qinghai-Tibet Plateau

Yu Zhu [1,2], Shiyin Liu [1,2]*, Miaomiao Qi [1,2], Ying Yi [1,2] , Wanqiu Li [3], Muhammad Saifullah [1,2], Sidou Zhang [1,2], Kunpeng Wu[1,2]

1 Yunnan Key Laboratory of International Rivers and Transboundary Eco-security,650091 Kunming, China; 2 Institute of International Rivers and Eco-Security, Yunnan University, 650091 Kunming, China; 3 College of Geodesy and Geomatics, Shandong University of Science and Technology, Shandong Qingdao 266590, China

* Correspondence: shiyin.liu@ynu.edu.cn;

Abstract: The eastern Qinghai-Tibet Plateau (EQTP) is the source regions of the Yangtze, Lancang/Mekong, and Nujiang/Salween rivers. Their hydrologic dynamics are key to water resources in the downstream area. An analysis of the spatiotemporal variations in terrestrial water storage (TWS) in this region has practical significance for regional social prosperity and the stability of the ecological environment. In this paper, the monthly GRACE Level 2 Release 6 (RL06) products were employed to invert TWS changes from April 2002 to August 2016, and dominant factors contributing to the changes in TWS in subbasins and decreasing and increasing areas were analyzed systematically. We concluded that. (1) the TWS in EQTP showed a slight decreasing trend from 2002 to 2016 with the obvious spatial heterogeneity. The TWS trend ranged from -0.94~0.91 mm/m with a decreasing trend in the southwest and an increasing trend in the north. The pattern in TWS is approximately similar to the change in soil moisture (ΔSM). (2) the decrease in TWS may be attributed to the increase of evapotranspiration, which has approximately increased by 53%, and increase of glacial ablation and reduction of precipitation in EQTP. Moreover, the decrease in evapotranspiration can partly explain the increase in areas with TWS increase. However, we speculated that the lakes supplemented by glaciers are the main cause of the regional changes in TWS. Glacial ablation is the dominant factor in the region where a substantial decrease in TWS is observed (an approximately 69% contribution). (3) the decrease in TWS mainly occurs in summer and is mainly due to the increase in evaporation in summer because of warming, increase in wind speed and decrease in the relative humidity. (4) the mass balance of glaciers was estimated indirectly based on the GRACE results, but a further study is needed to determine the specific process.

Keywords: TWS; GRACE; Spatiotemporal differentiation; Controlling factors

1 Introduction

The Qinghai-Tibet Plateau, the Earth's third pole, possesses water resources feed billion of

people downstream in China, India, Pakistan and other countries in the region(Pritchard, 2017; Shrestha et al., 2015; Q. Zhao et al., 2019). The temporal and spatial changes in its water storage capacity have a major impact on the social economic development and livelihood of the region. In the context of global climate change, the ablation of ice and snow in this region has accelerated and the land water cycle has undergone significant changes, particularly in the eastern region (EQTP). Glaciers, frozen soils, lakes and wetlands are key components involving in hydrologic processes associated with water resources sustainable development in EQTP. The region is controlled by the South Asian and East Asian monsoons, the subtropical westerly jets, and the Siberian high system. These factors, combined with the topographical characteristics of north-south trending high mountains and deep-incised valleys, create unique spatial and temporal differences in the characteristics of the terrestrial water cycle in EQTP. The region is characterized by the three river systems of Jinsha, Lancang and Nujiang in parallel from east to west (we here refer to the system as three parallel river basins (TPRB)) in the transition zone between the Qinghai-Tibet Plateau and the Yunnan-Guizhou Plateau. In recent years, EQTP has been attracted increasing attention from various sectors due to issues of the increased frequency and intensity of natural disasters, ecological degradation, and less social and economic development. Frequent natural disasters are mainly represented by large-scale and long-term droughts and regional floods. From the perspective of hydrology, an important cause of droughts and floods is an abnormality in terrestrial water dynamics. Many studies on drought and floods events in different basins (e.g., the Amazon basin (J. L. Chen, Wilson, Tapley, Yang, & Niu, 2009), Texas basin (Long et al., 2013), Haihe basin (J. Wang, Jiang, Huang, & Wang, 2014), and Liaohe basin (X. Chen, Jiang, & Li, 2018)) have shown that the spatial and temporal characteristics of regional water storage displayed varying degrees of abnormal fluctuations during the disaster period, and this abnormal fluctuation is generally linked to climate change (Forootan et al., 2019). The variability of TWS has been observed in EQTP, but the detailed characteristics of the fluctuations, the range of fluctuations and the spatial differences in the fluctuations remain unclear and must be elucidated.

The logistic constraints are always the challenge in traditional site-monitoring of TWS in basins with tough terrains though they can provide process data. Modeling practice for a large river basin is a measure to understand the interaction of various hydrological components and processes including droughts and floods, but these need as many measurements as possible for parameter validation and verification. Studies have reported that the TWS derived from Gravity Recovery and Climate Experiment (GRACE) satellite data showed potential both in revealing changes in surface water storage and ability supporting large scale hydrologic modeling (Frappart & Ramillien, 2018; Klees R 2006; Z. Luo, Yao, Li, & Huang, 2016; P. Yang, Xia, Zhan, Qiao, & Wang, 2017; K. Zhao & Li, 2017). As mentioned before, GRACE has applied in many river basins and has displayed satisfactory results in TWS changes (Feng et al., 2017; Khaki et al., 2018; W. LI et al., 2018; Ni et al., 2014; Qiong, Luo, Zhong, & Wang, 2013; L. Wang, Kaban, Thomas, Chen, & Ma, 2019; Zhen et al., 2018). The promising application can also be found for demonstration of TWS variability in the Three Gorges reservoir area, the Guanzhong Plain and some medium-scale

basins. The derived TWS from GRACE may benefit understanding TWS variability for rugged terrain basins like EQTP with large spatial relief and with limited in-situ measurements. The TWS data is also a treasure for the model validation and verification in these complex rivers.

The spatiotemporal characteristics of TWS and its change are results of the integrated effect of climate change and human activities (Hu, Liu, Bao, & El-Tantawi, 2018). Precipitation, runoff, and evapotranspiration are the dominating processes of changes in TWS either in space or in time (Frappart, Ramillien, & Ronchail, 2013; Tangdamrongsub, Hwang, & Kao, 2011; T. Yang, Wang, Chen, Chen, & Yu, 2015). Being one of active processes in rivers, the depletion of glaciers and snow cover is influential factor in TWS dynamics (Syed, Famiglietti, Rodell, Chen, & Wilson, 2008). As for anthropogenic processes like irrigation, abstraction of groundwater, land use, etc. also impact TWS in high populated area (de Beurs, Henebry, Owsley, & Sokolik, 2015; Huang et al., 2015; Khandu, Forootan, Schumacher, Awange, & Müller Schmied, 2016). According to a recent study, the dominant factor contributing to the increase in TWS in eastern India and southeastern Tibet was increased precipitation, while the decrease was mainly attributed to a decrease in precipitation and an increase in irrigation water (Rodell et al., 2018). Another study, however, pointed out that evapotranspiration dominates the TWS depletion in the Brahmaputra and precipitation played an important role on the TWS accumulation in the upper Yangtze, and additionally glacier mass loss was the most likely cause of TWS decrease in Brahmaputra (Meng, Su, Li, & Tong, 2019). Two findings show partly different dominated factors of TWS change in almost the same area (the most part of EQTP), which leads us to understand with uncertainty. The possible reasons account for it are different datasets used and different division of regions for exploring controlling factors. The latter may be more principal because each region has its own particular local climates, relief conditions and human conditions, and some factors affecting judgment will be involved if evaluating dominated factors in large scale region; for instance, in EQTP, human activities are less intensive and their impact on TWS can be ignored, but the widely distributed glaciers and snow in this area force us to consider the substantial impacts of snow and ice meltwater on TWS. Consequently, the controlling factors for variations in TWS should be further discussed with more validated datasets and detailed geographic division, especially in EQTP with complex relief condition. In order to clarify the spatiotemporal variation of TWS in EQTP and the controlling factors for such changes, based on the optimized data processing method and time series analysis, firstly, we get GRACE derived TWS in EQTP and describe the variations. Secondly, we divide EQTP into several parts according its geographical conditions and present the dominant factors associated with the increase and decrease in TWS throughout the region and in subbasins to provide references for local agriculture and animal husbandry and ecological water demand predictions and management. Section 2 describes the study area. In section 3, we detailed describe the datasets and methods we used. Section 4 presents the results and section 5 provides discussions of controlling factors in TWS variations. The study is summarized and concluded in section 6.

2 Study area

We defined EQTP as the region that covers the entire TPRB (90°E-101°E, 27°N-36°N) with an approximate area 1,207,400 km^2 (TPRB 399,000 km^2), including the sources of the Nujiang River, the Lancangjiang River, and the Jinshajiang River, as well as their basins in north of Yunnan province, and part of the big bend region at Brahmaputra (Figure 1). The part of Brahmaputra is included because there is glacierized area which may affect notably on the TWS change in the context of glacier retreat in high mountain Asia. The topography of the region is complicated, with an average altitude exceeding 3000 m, and the terrain fluctuates substantially, as it is generally high in the north and low in the south, high in the west and low in the east, and inclines downward from northwest to southeast. The study area is within the influence of the southwest monsoon and the southeast monsoon. It traverses the subtropical zone, the plateau temperate zone, and the plateau subfrozen zone from south to north, with substantial differences in climate. Its ecological environment and meteorological conditions are not only affected by the uplift of the Qinghai-Tibet Plateau but also affected by the formation and evolution of the longitudinal range-gorge. Dry-hot valleys surrounded by a relatively humid environment with a high temperature in this region are very common, such as the TPRB region (J. Guo, Wang, Bai, & Lu, 2006; Y. Luo, 2009). The soil in EQTP consists predominantly of sandy loam and loam. Loam soil is characterized by moderate loose and fine soil, a slow increase in temperature in spring, a good water storage capacity, and a good soil structure, while sandy loam has more sand and stones, blocks when dry, and a weaker water holding capacity than loam. The spatial differences in soil will cause a difference in the soil water holding capacity, which will affect the changes in TWS. Coupled with the complex terrain and varied climatic conditions, the spatial and temporal variability in water storage will be more prominent.

The unique environment and terrain make the region rich in water resources, mineral resources, biological resources, and tourism resources, which are closely related to human survival, development and resource development. The region has been suffering warming and drying in recent decades (T. Li, Wang, Chang, Zhang, & Li, 2018). A rise of 0.7 degrees Celsius in temperature and a reduction of 5.5 mm in area-averaged precipitation was posted in the latest 15 years. The arid climate has caused the region to suffer from frequent environmental problems, such as water shortage, grassland degradation, land desertification and soil erosion, which have further produced a series of vicious cycles (T. Li et al., 2018). Therefore, the temporal and spatial variations in TWS must be identified as an indicator of regional water resources and their responses to climatic events.

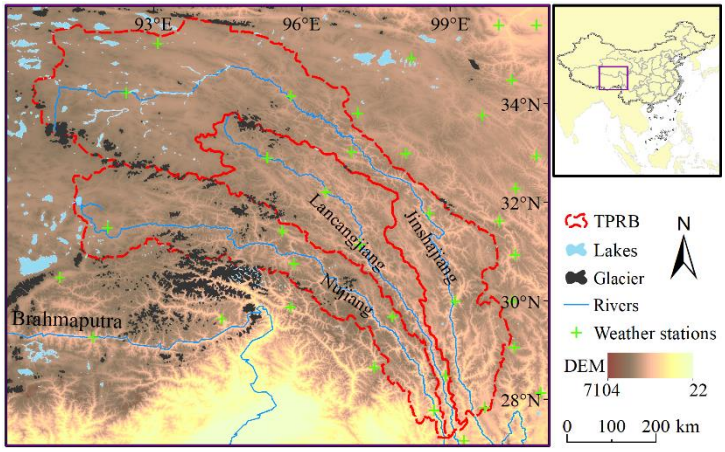

Figure 1. Study area mainly represented by TPRB and part of the Brahmaputra river basin. The locations of weather stations are shown.

3 Data and methods

3.1 Data

3.1.1 GRACE RL06

The GRACE satellite is a convenient and effective tool to obtain the highly precise temporal changes in the gravitational field at a particular moment. The data collected by the GRACE satellite have been applied in geodynamics, hydrology and other fields (Tapley, Bettadpur, Watkins, & Reigber, 2004). In this paper, GRACE LEVEL-2 (RL06) GSM (spherical harmonic coefficient of the geoid model) data produced by the Center for Space Research, University of Texas at Austin (UTCSR) were employed to calculate the TWS. The data were collected from April 2012 to August 2016, with a time resolution of 1 month, and the spherical harmonic coefficient of gravity was truncated to order 60. RL06 is still the same as RL05 in the form of expression, which mainly reflects the regularized spherical harmonic coefficient after deducting the influences of nontidal atmosphere and ocean masses, the influences of various tidal factors (including solid tide, sea tide, earth rotation polar tide, etc.) and the gravitational disturbances caused by the sun and moon (Bettadpur, 2018). However, some new background fields are adopted for RL06, and the processing method has been improved, resulting in a substantial reduction in error, particularly the error of the north-south strip (Gao, Lu, & Shi, 2019; Save, 2017).

The GRACE monthly gravity field model must be refined because of the error. The satellite laser ranging (SLR) C20 has a higher precision and is more sensitive in reflecting seasonal characteristics than GRACE. As a result, C20 of SLR is used to replace C20 of GRACE (J L Chen & Wilson, 2008; Cheng & Tapley, 2003). In addition, the improved p3m9 decorrelation filtering was used to eliminate the north-south strip error, and the 300 km fan filtering was used to reduce the high-order spherical harmonic coefficient error in the present study (Han et al., 2005; Zhen et al., 2018). After completing the procedure described above, the steady state quality of the Earth was estimated by calculating the monthly mean of the spherical harmonic coefficient, and the time-varying gravity data were obtained by deducting the steady state.

3.1.2 Hydrometeorological data

(1) Soil moisture data

The Global Land Data Assimilation System (GLDAS) datasets, established by the Goddard Space Flight Center (NASA) and the National Centers of Environmental Prediction (NCEP), were used in present study, which is proved to an efficient tool for examining meteorology and hydrology (Wu, Si, He, & Wu, 2019; Xia et al., 2014; P. Yang, Xia, Zhan, & Wang, 2018). GLDAS, including three land surface models (NOAH, CLM, and Mosaic) and one hydrological model (VIC), provides datasets (global precipitation, soil temperature, runoff, radiation flux and other hydrometeorological data) that are simulated based on multiple observation data, atmospheric assimilation products and reanalysis data for use by various researchers and relevant institutions (Rodell et al., 2004). The four-layer soil moisture data of NOAH have been widely used in the inversion of GRACE-derived TWS (W. LI et al., 2018; Zhen et al., 2018; Zhong et al., 2018). The data derived from NOAH from 2002 to 2016 were employed in this study, with a spatial resolution of 1°×1° and a temporal resolution of one month, and were mainly used to calculate the scale factor and characterize the soil moisture in the water balance.

(2) Precipitation data

As the largest input to the TWS, precipitation data are crucial for identifying the regional water balance process. Data from four grid models, CN501, TRMM.3b43v7, Global Precipitation Climatology Project (GPCP) and Precipitation Estimation from Remotely Sensed Information using Artificial Neural Networks-for Climate Data Record (PERSIANN-CDR), were used in this study. The accuracy of precipitation in EQTP was inter-validated with these precipitation data by comparison with the station data in the region and the bias corrected precipitation data was applied to describe the characteristics of the precipitation in EQTP (Figure 1). CN501 data include hourly and daily precipitation, temperature and evapotranspiration gridded at 0.25°×0.25° generated by interpolation based on observations over 2,400 meteorological stations in China (Jia & Xuejie, 2013). Trmm.3B43V7 is one of the datasets of Tropical Rainfall Measuring Mission Multisatellite Precipitation Analysis (TMPA), with a temporal resolution of 3 hours and a spatial resolution of 0.25° (Huffman et al., 2007). GPCP data are monthly precipitation at 1°×1° on the globe which was inversed from satellite data and verified by more than 6,000 meteorological stations around the world (Adler et al., 2018). Based on satellite data inversion results, PERSIANN-CDR are simulated by an artificial neural network algorithm with a spatial resolution of 0.25° and a temporal resolution of one day (Ashouri et al., 2015). In this paper, the nearest neighbor interpolation was used to obtain the results from the model for the corresponding sites, and R-square, Bias, RMSE and rRMSE were used to evaluate the accuracy of each application (Junzhi, A-Xing, & Zheng, 2012). As shown in Figure 2, CN501, TRMM.3b43v7 and GPCP all displayed a good correlation with the station data, which better reflects the characteristics of regional precipitation. Moreover, PERSIANN-CDR did not perform well in EQTP. Although the four kinds of data have a high precision for estimating precipitation, the precipitation estimates from CN501 and TRMM.3b43v7 are more accurate than the estimates obtained with the other two datasets.

From the perspective of RMSR and rRMSE, CN501 is closer to the actual observed value, which may be related to the data source of CN501. Considering the limited time sequence length of TRMM.3b43v7, we used the precipitation estimated using CN501 in the present study.

To minimize the error caused by different data sources, the data for temperature and evaporation were also obtained from CN501 in this study, based on the above analysis.

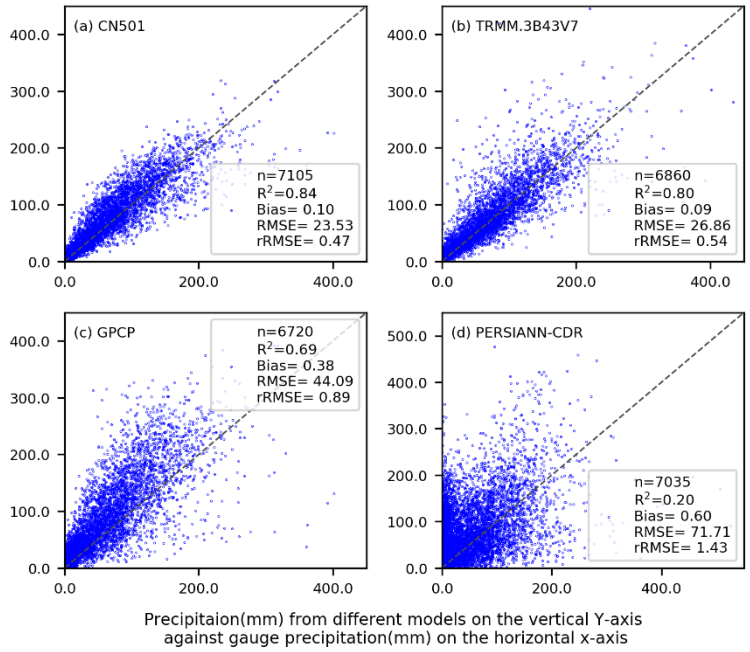

Figure 2. Comparative analysis of different gridded precipitation and measured data

(4) Runoff data

Runoff in the region is from the recent release of monthly global runoff data (GRUN) gridded at 0.5° by Gionata Ghiggi, which is a dataset simulated by machine learning based on data obtained from 35,002 sites (Ghiggi, Humphrey, Seneviratne, & Gudmundsson, 2019). The GRUN runoff variation of EQTP in 2002-2014 was calculated to be approximately 0.06 mm/m. According to the annual runoff depth of the basin published in the bulletin of Yunnan Water Resources (http://www.wcb.yn.gov.cn/list?code=xxgl2) from 2011 to 2015, we deduced that the trends for the variation in the surface runoff in Jinshajiang, Lancangjiang and Nujiang are approximately 16.16 mm/yr, -3.25 mm/yr and -21.97 mm/yr, respectively, and the equivalent water thickness (EWT) variation in the whole region is approximately 0.04 mm/m, weighted by basin area, smaller than GRUN because of the exclusion of runoff of Bramhmaputra River and some smaller water systems. However, compared with other hydrological simulation results (for example, the magnitude of GLDAS-NOAH runoff data in the study area is 10^{-6}-10^{-7} mm), GRUN is considered to be realistic and consistent in the research basins. Therefore, GRUN data were employed to depict regional runoff in the present study.

(5) Groundwater data

Underground logging can accurately reflect groundwater reserves, but the number of logging sites is small and data acquisition is difficult. In recent years, the data from WaterGAP Global

Hydrology Model (WGHM) simulated by IPG (University of Frankfurt) have better reflected the changes in groundwater reserves. In addition, the model also reflects the changes in all forms of water, except glaciers. Currently, the results from this model have been widely used (Eicker, Schumacher, Kusche, Döll, & Schmied, 2014; Feng, Shum, Zhong, & Pan, 2018). The groundwater data from the model were used in the present study, displaying a spatial resolution of 0.5°×0.5° and a temporal resolution of one month (Döll, Müller Schmied, Schuh, Portmann, & Eicker, 2015).

3.1.3 Measured data

To improve the validity and accuracy of the results, we derived the precipitation, evapotranspiration, wind speed, wind direction, temperature, humidity and other observation data recorded by 36 stations in the study area from the national meteorological center (http://data.cma.cn/) (Figure 1). After preprocessing the observed data, the time series of data recorded by 36 stations from 2002 to 2016 were obtained. The measured data from each station were mainly used to verify the accuracy of data obtained from the model and discuss the effects of meteorological factors on TWS.

3.2 Seasonal-trend decomposition procedure based on Loess (STL)

Since the data used in this paper are time series data, which can be decomposed to obtain details and to clarify the specific characteristics of changes in timing data. As a commonly used time-series decomposition method, STL is widely used in studies related to meteorology and hydrology. It divides the time series Y into a trend component T, periodic component (seasonal component) S and residual term R to refine and characterize variations in time series data at different levels (Cleveland & Cleveland, 1990; Rojo, Rivero, Romero-Morte, Fernandez-Gonzalez, & Perez-Badia, 2017; Sanchez-Vazquez, Nielen, Gunn, & Lewis, 2012). STL is divided into an inner cycle and outer cycle. The inner cycle is mainly used to fit the trend term and calculate the periodic components through detrending, subperiodic smoothing, subperiodic low-pass filtering, deperiodizing and trend smoothing. The outer cycle is mainly used to adjust the robustness of the weight in the fitting process to remove outliers (Cleveland & Cleveland, 1990). For time series Y, the STL decomposition at time i is calculated using equation (1):

$$Y_i = T_i + S_i + R_i \ \ (i = 1,2,\cdots,N) \tag{1}$$

In the present study, STL is mainly used to decompose time series data, such as TWS, and to analyze the characteristics of each component and extract effective information.

3.3 Inversion of TWS

One of the main explanations for the change in the spherical gravity field is the dynamic changes in the terrestrial water mass (Tapley et al., 2004), which is expressed in the form of EWT using the following equation (Wahr, Molenaar, & Bryan, 1998):

$$\Delta h(\theta,\lambda) = \frac{R\rho_e}{3\rho_w}\sum_{n=0}^{N}\frac{2n+1}{1+k_n}W_n\sum_{m=0}^{n}W_m(\Delta C_{nm}\cos m\lambda + \Delta S_{nm}\sin m\lambda)\bar{P}_{nm}(\cos\theta) \tag{2}$$

where R represents the mean radius of the Earth, with a value of 6.3781363×10^3 km. (θ,λ) refers to the geocentric latitude and longitude of the calculation points, respectively. ρ_e is the

average density of the earth, with a value of 5.517×10^3 kg/m^3, and ρ_w is the average density of water with a specific value of 1×10^3 kg/m^3. k_n denotes loading Love numbers, and both ΔC_{nm} and ΔS_{nm} are normalized spherical harmonic coefficients. $\bar{P}_{nm}(cos\,\theta)$ indicates the normalized m order n multiplied by the Legendre function. N is the order of the spherical harmonic coefficients. Studies have identified significant errors in the higher order terms. As a result, the higher order terms usually must be truncated. Generally, N=60 is used to calculate the EWT (Feng et al., 2013; Longuevergne, Scanlon, & Wilson, 2010; Swenson & Wahr, 2006). Both W_n and W_m are Gaussian filtering smoothing functions. When $r_{1/2}$ represents the filter radius, the Gaussian kernel function W is calculated using equation (3).

$$\begin{cases} W_0 = \frac{1}{2\pi}, W_1 = \frac{1}{2\pi}\left(\frac{1+e^{-2\alpha}}{1-e^{-2\alpha}} - \frac{1}{\alpha}\right), \dots, W_{n+1} = -\frac{2n+1}{\alpha}W_n + W_{n-1} & n>2 \\ \alpha = \frac{ln\,2}{1-cos(r_{1/2}/R)} \end{cases} \quad (3)$$

3.3.1 Recovery of the attenuated signal amplitude

Errors may also occur in a series of postprocessing operations of GRACE gravity field data (Klees R 2006), such as spherical harmonic expansion, spatial filtering (decorrelation filtering, fan filtering, etc.), which will cause leakage of the signal (Feng et al., 2017). Researchers have used several methods to address these errors. One is to simulate TWS through hydrological models and then perform postprocessing, consistent with GRACE to estimate signal leakage, which generally depends on the accuracy of hydrological models (Klees R 2006; Longuevergne et al., 2010). The other is the widely used scale factor method that employs the hydrological model to estimate the leakage ratio of a GRACE postprocessing step, which has been used to restore the real signal and reduce the dependence on the hydrological model to some extent. When the signal distribution in the research area is relatively uniform, the effect is better (Feng et al., 2017; Matthew, Isabella, & Famiglietti, 2009; Swenson & Wahr, 2007; Zhen et al., 2018). In addition, the regional mass change evaluation method based on spatial constraints is also applied to eliminate GRACE postprocessing errors (Feng et al., 2017; Jacob, Wahr, Pfeffer, & Swenson, 2012). Because some scholars obtained better inversion results using a single scale factor in the medium-scale research area (W. LI et al., 2018), the scale factor method was adopted to reduce the leakage error in this paper. Considering the seasonal characteristics and changing trend characteristics of the time series of TWS, STL decomposition was applied to the time series data before and after the filtering of TWS obtained by GLDAS, and the scale factors of a trend term and seasonal term (defined as double scale factors here) were calculated to recover the loss of signals. The scale factors of trend component and seasonal component are 1.14 and 1.05, respectively, and are used to recover GLDAS-derived TWS. The result is shown in Figure 3. The R^2 is approximately 0.99 for the comparison between before and after recovery. Except for individual peaks, TWS is generally consistent before and after the filter, indicating that the use of double scale factors better recovers the signal amplitude attenuation of TWS. Thus, we used this method to reduce the effect of the filter on TWS in the experiment.

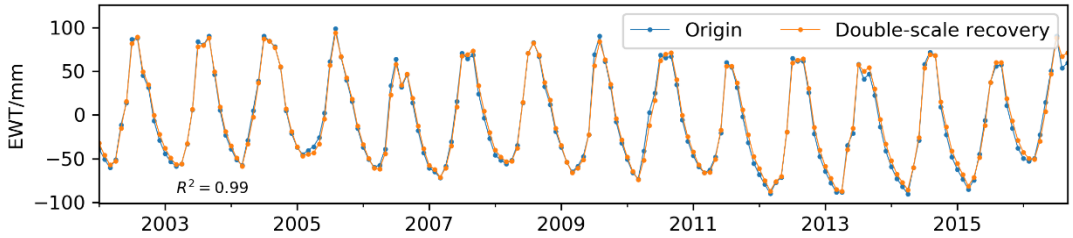

Figure 3. GLDAS-derived TWS before and after recovery of the double scale factors.

3.3.2 Water Balance

In the vertical direction, regional TWS includes surface runoff (SR), groundwater (GW), soil moisture (SM), melting water (including snow melting water (SW) and glacier melting water (G)), and the biological water content (Cao, Nan, & Cheng, 2015). The variation in the biological water content is relatively small and was ignored in the present study. Therefore, we did not consider the conversion process of SR, SM, GW, SW and G, and thus the changes in TWS in the study area were roughly measured by calculating changes in soil water (ΔSM), groundwater (ΔGW), runoff (ΔSR), snow melting (ΔSW) and glacier melting (ΔG).

Furthermore, from the perspective of the water cycle, the variation in TWS $\frac{d_{Tws}}{d_t}$ can also be denoted by changes in precipitation ΔP, evaporation ΔET and runoff ΔSR (Chao & Wang, 2017; D. Yang, Yang, & Lei, 2014). Considering the extensive snow and ice cover in the study area, snow melt water (SW) and glacier melt water (G) must be considered. The hydropower stations of Nujiang and Lancangjiang are mainly concentrated in the middle and lower reaches of the basins; hence, reservoir filling in the study area does not exert an effect on the results. Although a plan to established eight hydropower stations in the upper reach of Jinshajiang has been proposed, only three have been implemented up to 2016 and the scale is relatively small. For Bramhmaputra, no large reservoir is located in the study area. Therefore, the impacts of reservoirs in the study area have been ignored. Additionally, after ignoring some subtle hydrological processes, $\frac{d_{Tws}}{d_t}$ was calculated using formula (4). These variables and temperature are the main parameters used to analyze the changes in TWS.

$$\frac{d_{Tws}}{d_t} = \Delta P + \Delta SW + \Delta G - \Delta ET - \Delta SR \quad (4)$$

4 Results

4.1 The overall trend of TWS in EQTP

Using the TWS inversion methods described in section 3.3, the GRACE data were processed to obtain the water storage EWT of EQTP. As shown in Figure 4, the TWS showed a decreasing trend from 2002 to 2016, with an approximate rate -0.15 mm/m, but showed an increasing trend from 2002 to 2005, with an approximate rate 0.89 mm/m. The time series was decomposed to the trend item, seasonal item and residual item with STL to refine the characteristics of TWS. The seasonal variation in TWS was distinguished from the decomposed signal, which showed

substantial annual losses in winter and spring and the largest annual surpluses in summer and autumn. Its amplitude was maintained at ±50 mm, and no significant interannual variation in the seasonal characteristics was observed. The characteristics of changes in the trend term was basically consistent with the overall change in TWS, indicating that the change in TWS mainly depends on the trend term. The residual term of TWS reflects the characteristics of TWS fluctuations and is the most powerful evidence for drought or flood events in the region. No obvious pattern of fluctuations in TWS was observed, but obvious abnormal signals were detected, such as in the spring of 2003 and 2004, the winter of 2006 and 2015, etc. We counted the annual fluctuations in TWS to more intuitively show the surplus and deficits in TWS, and the results are shown in Table 1. In general, except for individual years, the loss of the water storage capacity is greater than 35 mm, resulting in a drying condition; however, the surplus of water reserves is maintained at greater than 30 mm. These findings are consistent with the characteristics of a dry-hot valley. Regarding the balance of TWS, losses were observed for 7 years from 2003 to 2015, particularly in 2004, 2006 and 2011. According to the statistics from the China Meteorological Disaster Yearbook issued by the China Meteorological Administration, the drought in the northern Yunnan and southeastern Tibet was severe in these years, and the agriculture and animal husbandry were substantially affected. Therefore, we affirmed that the losses of TWS in these years were related to droughts. From the peak of TWS surplus and deficit, except for 2003, 2004, 2008, 2010 and 2015, the largest losses in other years appeared in the summer and autumn, results that are completely opposite to the seasonal variation in TWS. We speculated that in these years, the study area experienced a certain degree of drought. More interestingly, in 2012 and 2014, the maximum deficit and maximum surplus appeared only one month apart, which may be caused by the lag of heavy precipitation on regional soil moisture supplementation.

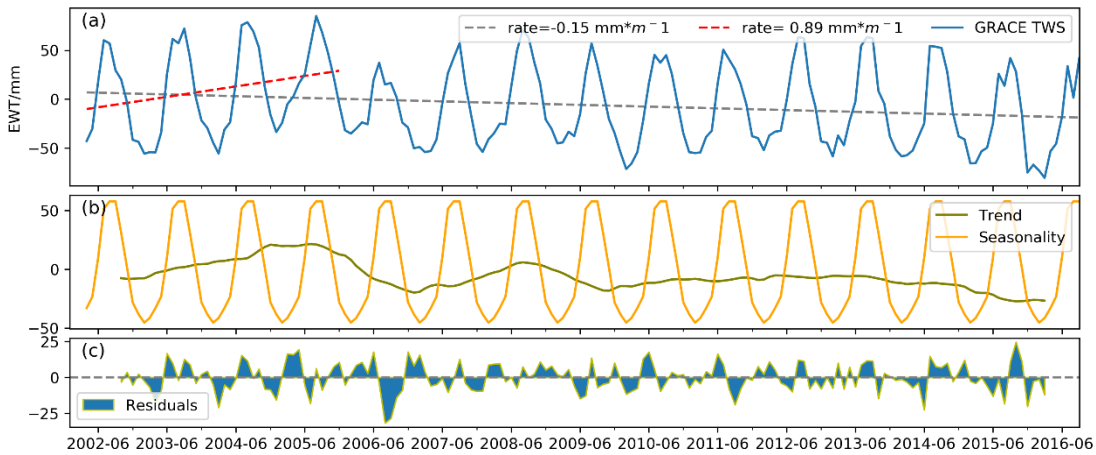

Figure 4. GRACE-derived TWS time series and characteristics of its composition.

Table 1 Characteristics of fluctuations in TWS

year	Surplus(mm)	Deficit(mm)	Budget(mm)	max surplus date	max deficit date
2003	52.47	42.29	10.19	2003-06	2003-04
2004	37.04	57.37	-20.33	2004-07	2004-03

2005	77.00	47.87	29.13	2005-05	2005-07
2006	59.49	92.48	-32.98	2006-12	2006-08
2007	40.19	44.85	-4.66	2007-02	2007-07
2008	53.39	19.75	33.64	2008-11	2008-01
2009	39.58	48.67	-9.10	2009-08	2009-06
2010	42.57	43.04	-0.47	2010-06	2010-02
2011	30.49	50.38	-19.90	2011-06	2011-09
2012	49.15	37.38	11.77	2012-08	2012-07
2013	52.56	36.87	15.69	2013-08	2013-10
2014	42.84	42.45	0.39	2014-07	2014-06
2015	58.58	65.55	-6.97	2015-10	2015-12

4.2 Spatial differences in TWS in EQTP

To understand the spatial differentiation of TWS in EQTP, we next performed a grid-to-grid process to obtain the long-term trend, which is defined as monthly average rate of TWS change (TWS) here. As shown in Figure 5, overall, the spatial variation rate of TWS ranged from -0.94 to 0.91 mm/m (the loss in local areas exceeded 1.4 mm/m). The spatial differences were significant. The southwest direction showed a large decreasing trend (defined as R1, the blue line frame in Figure 5), which is mainly the flow area of Brahmaputra River, and the north direction showed an increasing trend (defined as R2, the yellow line frame in Figure 5), particularly in the area recognized as the source of the Jinshajiang Basin. TWS in the central and eastern parts of the study area (defined as R3, between the blue line and the yellow line in Figure 5) changed slightly and generally maintained a balance. In addition, TWS in the middle and lower reaches of the TPRB experienced a significant loss that was largely related to unique topography of a typical dry-hot valley. This loss has led to frequent large-scale drought events in recent years. In TPRB, the overall performance of the Jinshajiang Basin was an increasing trend with a rate of 0.19 mm/m, and a weak downward trend was observed downstream of the basin. The headstream of the Lancangjiang Basin showed a slight increase in TWS; nevertheless, the TWS of the whole basin generally decreased at a rate of 0.28 mm/m. Nujiang Basin experienced a vast deficit in TWS and its negative change rate reached 0.49 mm/m.

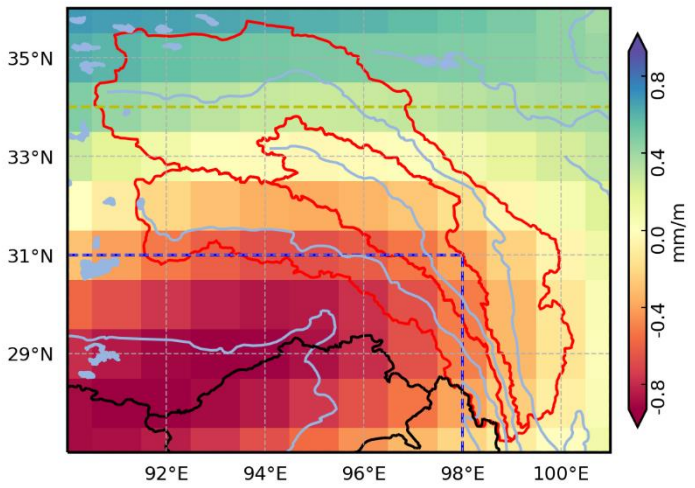

Figure 5. Map of the spatial distribution of changes in TWS in EQTP. The study area is divided into 3 parts by the yellow line and blue line, which are defined as R2, R3 and R1 from north to south, respectively.

5 Discussion

5.1 Partitioning components in TWS dynamics

Due to the limited amount of measured data, data from hydrological models were used to further explore the characteristics of variations in each component of TWS. Among these models, SM adopts data from the GLDAS-NOAH model, SR adopts data from the GRUN model, and GW uses WGHM results. As shown in Figure 6, the regional GW does not display an obvious trend of change, consistent with the results reported by Feng and colleagues (Feng et al., 2018), who showed that GW is not the main component contributing to the regional change in TWS. The change in SW tends to be 0, which is mainly because the snow and ice in the area are mainly concentrated in the upstream areas of the basins, and the area covered by ice and snow is much smaller than total area of EQTP. Regarding the whole area, the contribution of SW to changes in TWS is small, but the amount of change is generally greater than 0 (approximately 0-2 mm), particularly after 2011, indicating that the snow melt in basins is increasing. A continuous time series data representation for the change in glacier melt water is not available. However, according to previous studies, the glacier in EQTP has shown a negative mass balance in recent years, namely, the glacier melt water is increasing (Berthier, Cabot, Vincent, & Six, 2016; Kääb, Treichler, Nuth, & Berthier, 2015; Zhou, Li, Li, Zhao, & Ding, 2018). The changes in SR and SM are basically consistent with TWS, particularly after 2011, when the change in SM is larger. Therefore, SM is the main component of TWS. SM is a necessary condition for the survival and growth of regional plants. Drought occurs once SM is unable to meet the needs of plant growth. In 2009-2014, southwestern China, particularly in the Yunnan-Guizhou Plateau, continued to experience a drought (RONG Yanshu, 2018), and the drought was most severe in 2010. As shown in Figure 6, the extent to which the SM decreased during this period was large. Consequently, we inferred that the drought during this period was mainly caused by insufficient soil moisture.

Notably, in the southwestern drought in 2010, the reduction in TWS was large, while SM did not fluctuate substantially, and its rapid decrease occurred in early 2011. This difference may be caused by the lag effects of precipitation and evaporation on soil moisture. The decrease in the soil water content in 2011-2015 is greater than TWS. According to Zhang, an increase in the surface temperature enhanced regional evaporation, so the strengthened drought during the period (Zhang, Wang, Huang, Hao, & Duan, 2015). At the same time, due to the increasing temperature, the melting of glaciers was accelerated. Thus, we speculated that the acceleration of glacial ablation and the increase in evaporation partially contributed to the changes in TWS in the southwest of the region.

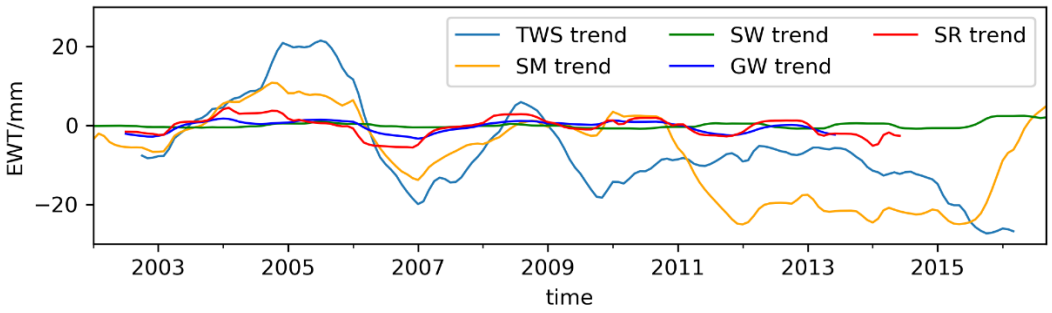

Figure 6. Trends of changes in TWS and its components

5.2 Attributes of spatial heterogeneity in TWS

In this section, we analyze the causes of spatial differences in water reserves based on changes in precipitation, evaporation, melt water from ice and snow, runoff, etc. The TWS in R3 remained stable and will not be discussed here. We mainly analyzed the entire study area and zones R1 and R2.

Based on the results described above, the loss rate of the entire region was 0.15 mm/m for the study period. As the change in SW tends to be 0, the contributions of precipitation, evaporation and runoff to TWS are mainly discussed here. The variability in evaporation in the region is 0.0876 mm/m, the variability in precipitation is -0.0334 mm/m, and the variability in runoff is 0.0078 mm/m (which was not considered a substantial change) (Figure 7(a)). According to formula (5), the regional glacial meltwater variability is -0.0212 mm/m. Because continuous time series data are not available to verify the glacial variability, this paper uses the results reported by Brun and colleagues (Brun, Berthier, Wagnon, Kaab, & Treichler, 2017) for validation. Brun reported a mass balance of representative glaciers in the study area of -0.62±0.23 m w.e.yr^{-1}. Ignoring the inconsistency of glacial changes, we used -620 mm/yr for the water equivalent of the glacier changes in the study area. The area of glaciers in the study area is approximately 7342.79 km^2, as extracted by the Second Glacier Inventory Dataset of China (Version 1.0) (W. Guo et al., 2015; Wanqin et al., 2014) , and the melting rate of glaciers in the study area is approximately calculated as -0.31 mm/m from the area ratio. We concluded that a substantial difference exists between the two results, and the rate of variations in glacial melt water in the study by Brun and colleagues is even higher than the TWS. One of the main explanations is that most of glacial melt

water will flow into the lakes, particularly in EQTP with a large number of lakes, leading to a small regional mass loss caused by glacial melting. Therefore, from the perspective of the regional water balance, the results of this paper may better reflect the contribution of glaciers to the change in regional TWS. According to the variability of each parameter, the increase in evaporation is the main reason for the decrease in regional TWS (a contribution of approximately 53%), and the contributions of glacial ablation and reduced precipitation are approximately the same.

R1 is the area displaying a severe TWS deficit, with a loss rate of -0.71 mm/m. As shown in Figure 7(b), the decrease in regional precipitation decreases and the increase in evaporation are similar to the entire region, except that the precipitation (-0.0930 mm/m) and the evaporation (0.1912 mm/m) exhibit higher variability. Moreover, regional runoff displays a decreasing trend, but the variation rate is small (-0.0026 mm/m) and can generally be ignored. Similarly, the variability in glacial meltwater calculated using formula (5) is approximately -0.43 mm/m. Based on the results reported by Brun et al., we concluded that the glacial melt variability in R1 is approximately -0.64 mm/m (the glacier area is 4368.836 km^2, and the water equivalent of the glacial melt is 620 mm/yr). A noticeable difference is observed between the two results. One explanation for the difference is that the mass balance is quite different for different glaciers in this area, based on the mass balance observations reported by Yang and colleagues (W. Yang et al., 2010). When the upper limit of the error term of the result reported by Brun and colleagues is considered, the results are basically consistent with the calculated value reported in this paper. Based on the variability in each variable, glacial melting in R1 is the main reason for the decrease in TWS, and the contribution is 61%. Additionally, the increase in evaporation contributes substantially to the decrease in TWS. The decrease in precipitation exerts an insignificant effect on the reduction in TWS.

R2 is the area showing an increase in TWS, with a rate of 0.49 mm/m. As shown in Figure 7(c), although the regional precipitation and runoff increase and evaporation decrease, the extent of these changes is small. The contribution of the three parameters to the increase in TWS is no more than 5%. According to formula (5), the variability in glacial melt water is approximately 0.46 mm/m, which is obviously inconsistent with the actual situation. Figure 1 shows the presence of many large lakes in R2. According to relevant research, the water volume of lakes in the Qinghai-Tibet Plateau has increased significantly in recent years, and many new lakes have appeared (X. Li et al., 2019). Therefore, the contribution of the increase in lake water storage to the change in TWS must be considered. Currently, detailed data are not available to obtain the amount of change in the water storage capacity of these lakes, and thus we can only speculate that the increase in TWS observed in this area is closely related to lake expansion. The recharge source of these lakes is mainly the glaciers in R2 and those located outside the study area, which indirectly shows that glacial changes contribute to the increase in TWS. Considering the mechanism of the production and convergence of glacial meltwater, we speculated that the rate of ablation of glaciers in this region is higher than in R1. In addition, in recent years, the depth of the frozen soil active layer on the Tibetan Plateau has significantly increased, and the freezing depth

has decreased significantly (Peng, 2018; W. Zhang et al., 2015). From this perspective, the transfer of mass from the ablation of frozen soil around the study area may also affect the changes in TWS.

In TPRB, the changes in TWS show different characteristics in sub-basins, which are caused by different factors. Thus, the dominant factor contributing to TWS fluctuations in each sub-basin is simply analyzed here. As shown in Table 2, the precipitation in three sub-basins of TPRB displays a decreasing trend, and both evaporation and runoff are increasing. Considering the low-level effects of snow and ice melt water, the increase in evaporation is the main cause of the decrease in TWS in Lancangjiang and Nujiang. In the Jinshajiang Basin, the variability in precipitation and evaporation is comparable. Based on a previous analysis, the expansion of lakes in this basin is a possible cause of the increasing TWS. After ignoring the change in snow melt water, the variability of glacial meltwater in the Lancangjiang and Nujiang Basins were calculated to be -0.13 mm/m and -0.27 mm/m, respectively. The change in TWS caused by the expansion of the lakes is unable to be deduced at present, and thus the variability in the melt water of the Jinshajiang Basin is not discussed here. The melting of glaciers exerts a substantial effect on the changes in TWS in two basins, particularly in the Nujiang Basin (the contribution rate to TWS is equivalent to the sum of precipitation, evaporation and runoff contribution rates). As the temperature of the whole region continues to increase, the melting of ice and snow will accelerate and the evaporation will substantially increase. We predict that the degree of dry conditions and heat in this area will become more obvious in the future, and the TWS will continue to decrease, which will substantially affect the production and living water available in TPRB.

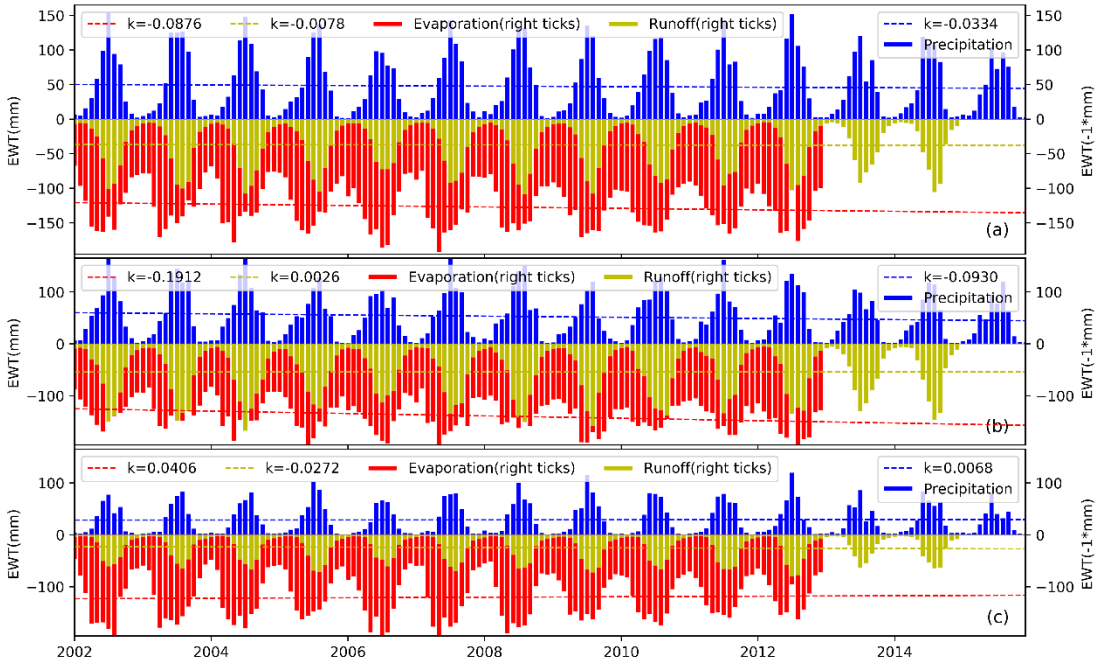

Figure 7. Time series of precipitation, evaporation and runoff in the entire study area (a), R1 (b) and R2 (c).

Table 2. Rates of changes in precipitation, evaporation, runoff in the sub-basins of TPRB (unit: mm/m).

Basins	TWS	ΔP	ΔE	ΔSR	ΔG
Jinshajiang	0.19	-0.04	0.04	0.02	—
Lancangjiang	-0.28	-0.02	0.10	0.03	-0.13
Nujiang	-0.49	-0.06	0.15	0.01	-0.26

5.3 Factors affecting the decrease in TWS in summer

Based on the analysis described above, the increase in evaporation is the main cause of the decrease in TWS in EQTP during the study period. Additionally, the decrease in precipitation also contributes to the decrease to some extent. Generally, of all seasons, the highest levels of evaporation are observed in the northern regions during the summer (defined as June, July and August, and represented by Q3) (Su & Feng, 2015), when the study area is also significantly affected by the Indian Summer Monsoon. Therefore, in this section, we will discuss the changes in TWS in the northern region during the summer and the factors that substantially influence evaporation. Namely, whether the variations in air temperature, air humidity and wind speed converge with the characteristics of changes in evaporation. We will also analyze the variations in the Indian Summer Monsoon and its feedback effect on precipitation to analyze the factors that affect the change in TWS in the northern region during the summer.

As shown in Figure 8, it's observed that water deficit in summer dominates the annual trend in TWS in the northern region. Meanwhile, precipitation shows a decreasing trend that converges with the varying trends of TWS. Although the rate of decrease in precipitation is small, as the main component of the regional water reserves, this small decreasing rate slows the loss of TWS. Precipitation varies substantially in regions with complex topographic conditions, but based on the time series data, changes in precipitation are mainly affected by atmospheric conditions, and topographic and geomorphic features are only amplifiers of atmospheric conditions. In the northern region during summer, the study area is mainly affected by the Indian Summer Monsoon (Yao et al., 2017), and thus we used the Indian Monsoon Index (IMI) (B. Wang & Fan) to measure the relationship between the Indian Summer Monsoon and precipitation during the study period. In Figure 8, the IMI exhibits a decreasing trend, indicating that the IMI is weakening and the moisture brought by the Indian Summer Monsoon is decreasing during this period, which is a definite reason for the overall decrease in regional precipitation. Based on the characteristics of the change, IMI is more consistent with the change in TWS than the change in precipitation. After the summer of 2005, the Indian Summer Monsoon has weakened continuously, but the precipitation only decreased slightly with a larger interannual fluctuation in general, which was particularly large from 2011 to 2015. Thus, the weakening of the Indian Summer Monsoon is not the main cause of the decrease in precipitation in EQTP, which requires further research and we will not delve into this topic in the present study. However, we speculate that the increases in summer temperature and evaporation (Figure 9), together with the changes in underlying surface in the region (the decrease in vegetation cover caused by human activities and the decrease in glacier cover area caused by warming in the region, etc.), result in a decrease in the atmospheric water vapor content, which may be another explanation for the regional decrease in precipitation.

As shown in Figure 9, evaporation is the main factor contributing to the decrease in TWS and increased significantly in summer, with a higher trend than observed throughout the year. Based on these findings, the regional decrease in TWS that is mainly observed in summer is generally

controlled by the increase in evaporation. To clarify the reasons for the increasing evaporation in summer, we selected the meteorological elements with a greater impact on evaporation in the region and analyzed their changes. Generally, during the study period, the air temperature increased, the wind speed increased, and the air humidity decreased, consistent with the variation in evaporation in the region. Air temperature, wind speed and relative humidity all contribute to the increase in evaporation in some extent. In terms of the rate of change, the change in relative humidity has the greatest contribution to the evaporation, followed by the wind speed. However, the relative humidity is also affected by the changes in temperature and air pressure. Therefore, the extent of the contributions of the three factors to evaporation is difficult to determine. Nevertheless, in terms of the fluctuations, we determined that changes in temperature were the most consistent with changes in evaporation, indicating that changes in temperature are the factor with the greatest direct effect on evaporation. As shown in Figure 9, the change in regional evaporation is consistent with the change in TWS, but the temperature is consistent with TWS due to a lag. Regarding the points at which evaporation and temperature changed in the time series data, asynchronous correlations were observed between two variables as well, indicating that the temperature change exerted a certain lag effect on evaporation.

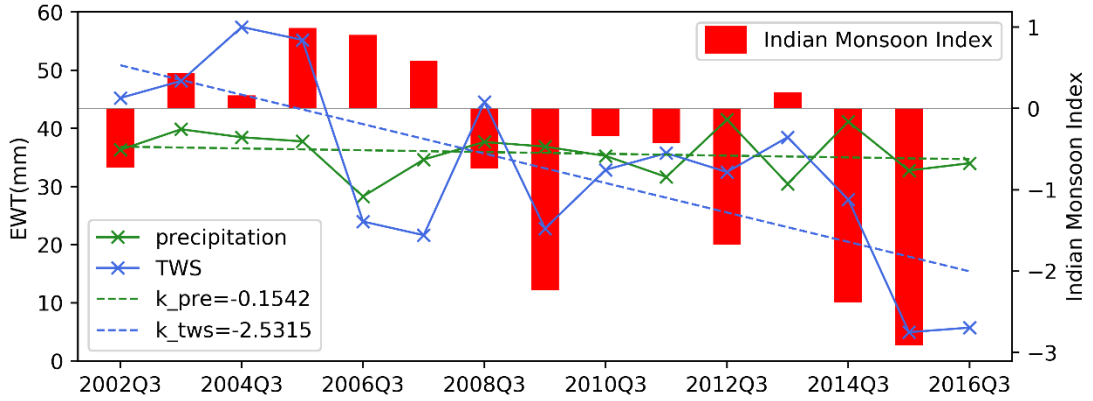

Figure 8. Changes in TWS, precipitation and IMI in summer.

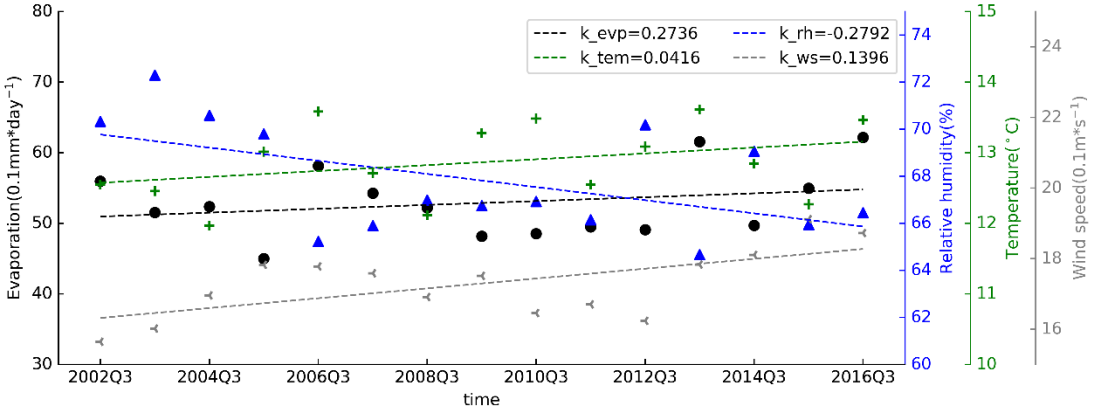

Figure 9. Changes in evaporation, relative humidity, temperature and wind speed in summer.

6 Conclusions

Natural disasters, such as droughts and floods, in EQTP are closely related to changes in TWS. In response to these changes, the paper uses data from multiple sources to invert the TWS and determine the characteristics of its changes. The characteristics of the temporal and spatial variations in TWS and their correlations with regional drought events were quantitatively analyzed. Moreover, we clarified the reasons for the spatiotemporal differences in TWS. Overall, we have obtained the conclusions listed below.

(1) Overall, from 2002 to 2016, the TWS in EQTP shows a slight decreasing trend, and the spatial differences are significant. The spatial change rate ranges from -0.94 to 0.91 mm/m, and shows a decreasing trend in the southwest and an increasing trend in the north. Although the TWS decreased overall, an increasing trend was observed from 2002 to 2005, with a rate of 0.89 mm/m. In addition, the seasonal changes in TWS are remarkable, with an amplitude of ±50 mm. The effective signals intuitively reflect the fluctuations in the income and expenditure for TWS. Based on the statistical analyses, except for individual years, the loss of TWS exceeds 35 mm/yr. In 2004, 2006 and 2011, the TWS experienced serious losses. In the years when droughts occurred, TWS was abnormally fluctuating. Among the subbasins, the Nujiang Basin experienced a substantial loss of TWS; Jinshajiang Basin had a surplus of TWS, particularly in the source area and its northwest direction; the Lancangjiang Basin basically maintains a balance of water reserves; and the Brahmaputra Basin in the study area is the area with the most serious loss.

(2) ΔSM is the main component of TWS, and the characteristics of the variation in this parameter are the same as TWS. In the whole region, ΔSR, ΔGW and ΔSW exert little effect on TWS, and the contribution of ΔG is unclear because of the lack of available continuous glacier change data. From 2006 to 2015, SM was in a loss state, and ΔGW and ΔSW changed more than 0 in the corresponding period. Consequently, the continuous decrease in SM was the main cause of the drought event during this period. Although the contribution of ΔSW to the change in TWS is small, it presents distinct peaks during the dry season that are related to the negative mass balance of glaciers. GW fluctuates substantially during the dry season, particularly in the years of persistent droughts, indicating that the occurrence of drought disasters exerts a greater impact on regional GW. The effect of ΔSR on the change in TWS is somewhat different in each sub-basin.

(3) In terms of the factors controlling the changes in TWS, the increase in evaporation is the dominant factor contributing to the decrease in TWS in EQTP (a contribution of approximately 53%), while the contributions of glacial ablation and reduced precipitation to changes in TWS are basically equivalent. In the area where water reserves are increasing (region 2), evaporation plays a leading role in contributing to changes in TWS among precipitation, evaporation and runoff, but the total contribution of the three factors is relatively low. We speculated that expansion of lakes replenished by glaciers is the main reason for the change in regional TWS. In the area (R1) displaying a loss of TWS, glacier ablation is the main contributing factor (a contribution of approximately 61%). Additionally, evaporation has more significant contribution than precipitation, although the increase in evaporation and the decrease in precipitation affect the decrease in TWS.

(4) The decrease in TWS mainly occurs in summer. The increase in evaporation in summer is the main cause of the decrease in TWS. Additionally, the decrease in precipitation, which serves as the input of TWS, also plays a role. The increase in evaporation in summer is the result of an increase in temperature, an increase in wind speed and a decrease in relative humidity. The Indian Monsoon exerts a certain effect on the decrease in summer precipitation, but the dominant factor contributing to the decrease requires further study.

(5) The application of GRACE-derived TWS combined with accurate precipitation, evaporation, runoff and other data allowed us to indirectly estimate the glacier mass balance in the basin, but the accuracy of the results largely depends on completely separating the effects of underlying surface factors of the basin, such as lakes, reservoirs and permafrost.

Acknowledgements: The authors thank members of Institute of International Rivers and Eco-Security, Yunnan University, plus Fuming Xie, Yongpeng Gao, Wenfei Miao, Xinxin Qiang and Shimei Duan for their input and stimulating discussions over past few months. We also thank Dr. Wei Feng at Institute of Geodesy and Geophysics, Chiese Academy of Sciences for helpful comments on this manuscript. This work is supported by the National Natural Science Foundation of China (No. 41761144075 and No. 41661144044), the Research Funds for Introducing Talents of Yunnan University (No. YJRC3201702) and Innovation Fund Designated for Graduate Students of Yunnan University (Grant No. 2018Z099).

Data Availability Statement: The data that support the findings of this study are available from the corresponding author upon reasonable request.

Author Contributions: In this paper, Shiyin Liu and Yu Zhu conceived and designed the experiments. Yu Zhu performed the analysis and drafted the first manuscript, and Shiyin Liu and Yu Zhu discussed and improved the first version. All authors involved in the discussion of the results and revision of the manuscript.

Conflicts of Interest: The authors declare no conflicts of interest.

References

Adler, R. F., Sapiano, M., Huffman, G. J., Wang, J., Gu, G., Bolvin, D., . . . Shin, D. B. (2018). The Global Precipitation Climatology Project (GPCP) Monthly Analysis (New Version 2.3) and a Review of 2017 Global Precipitation. *Atmosphere (Basel), 9*(4). doi:10.3390/atmos9040138

Ashouri, H., Hsu, K.-L., Sorooshian, S., Braithwaite, D. K., Knapp, K. R., Cecil, L. D., . . . Prat, O. P. (2015). PERSIANN-CDR: Daily Precipitation Climate Data Record from Multisatellite Observations for Hydrological and Climate Studies. *Bulletin of the American Meteorological Society, 96*(1), 69-83. doi:10.1175/bams-d-13-00068.1

Berthier, E., Cabot, V., Vincent, C., & Six, D. (2016). Decadal Region-Wide and Glacier-Wide Mass Balances Derived from Multi-Temporal ASTER Satellite Digital Elevation Models. Validation over the Mont-Blanc Area. *Frontiers in Earth Science, 4*. doi:10.3389/feart.2016.00063

Bettadpur, S. (2018). *Gravity Recovery and Climate Experiment Level-2 Gravity Field Product User Handbook*: Center for Space Research at The University of Texas at Austin.

Brun, F., Berthier, E., Wagnon, P., Kaab, A., & Treichler, D. (2017). A spatially resolved estimate of High Mountain Asia glacier mass balances, 2000-2016. *Nat Geosci, 10*(9), 668-673. doi:10.1038/NGEO2999

Cao, Y., Nan, Z., & Cheng, G. (2015). GRACE Gravity Satellite Observations of Terrestrial Water

Storage Changes for Drought Characterization in the Arid Land of Northwestern China. *Remote Sensing, 7*(1), 1021-1047. doi:10.3390/rs70101021

Chao, N., & Wang, Z. (2017). Characterized Flood Potential in the Yangtze River Basin from GRACE Gravity Observation, Hydrological Model, and In-Situ Hydrological Station. *Journal of Hydrologic Engineering, 22*(9), 05017016. doi:10.1061/(asce)he.1943-5584.0001547

Chen, J. L., & Wilson, C. R. (2008). Low degree gravity changes from GRACE, Earth rotation, geophysical models, and satellite laser ranging. *Journal of Geophysical Research Solid Earth, 113*(B6), -.

Chen, J. L., Wilson, C. R., Tapley, B. D., Yang, Z. L., & Niu, G. Y. (2009). 2005 drought event in the Amazon River basin as measured by GRACE and estimated by climate models. *Journal of Geophysical Research, 114*(B5). doi:10.1029/2008jb006056

Chen, X., Jiang, J., & Li, H. (2018). Drought and Flood Monitoring of the Liao River Basin in Northeast China Using Extended GRACE Data. *Remote Sensing, 10*(8), 1168. doi:10.3390/rs10081168

Cheng, M. K., & Tapley, B. D. (2003). Variations in the Earth's Oblateness During the Past 26 years. *Journal of Geophysical Research Solid Earth, 109*(9), 1404-1406.

Cleveland, R. B., & Cleveland, W. S. (1990). STL: A seasonal-trend decomposition procedure based on loess. *Journal of Official Statistics, 6*(1), 3-33.

de Beurs, K. M., Henebry, G. M., Owsley, B. C., & Sokolik, I. (2015). Using multiple remote sensing perspectives to identify and attribute land surface dynamics in Central Asia 2001–2013. *Remote Sensing of Environment, 170*, 48-61. doi:10.1016/j.rse.2015.08.018

Döll, P., Müller Schmied, H., Schuh, C., Portmann, F. T., & Eicker, A. (2015). Global-scale assessment of groundwater depletion and related groundwater abstractions: Combining hydrological modeling with information from well observations and GRACE satellites. *Water Resources Research, 50*(7), 5698-5720.

Eicker, A., Schumacher, M., Kusche, J., Döll, P., & Schmied, H. M. (2014). Calibration/Data Assimilation Approach for Integrating GRACE Data into the WaterGAP Global Hydrology Model (WGHM) Using an Ensemble Kalman Filter: First Results. *Surveys in Geophysics, 35*(6), 1285-1309. doi:10.1007/s10712-014-9309-8

Feng, W., Shum, C., Zhong, M., & Pan, Y. (2018). Groundwater Storage Changes in China from Satellite Gravity: An Overview. *Remote Sensing, 10*(5). doi:10.3390/rs10050674

Feng, W., Wang, C. Q., Da-Peng, M. U., Zhong, M., Zhong, Y. L., & Hou-Ze, X. U. (2017). Groundwater storage variations in the North China Plain from GRACE with spatial constraints. *Chinese Journal of Geophysics*.

Feng, W., Zhong, M., Lemoine, J.-M., Biancale, R., Hsu, H.-T., & Xia, J. (2013). Evaluation of groundwater depletion in North China using the Gravity Recovery and Climate Experiment (GRACE) data and ground-based measurements. *Water Resources Research, 49*(4), 2110-2118. doi:10.1002/wrcr.20192

Forootan, E., Khaki, M., Schumacher, M., Wulfmeyer, V., Mehrnegar, N., van Dijk, A., . . . Mostafaie, A. (2019). Understanding the global hydrological droughts of 2003-2016 and their relationships with teleconnections. *Sci Total Environ, 650*(Pt 2), 2587-2604. doi:10.1016/j.scitotenv.2018.09.231

Frappart, F., & Ramillien, G. (2018). Monitoring Groundwater Storage Changes Using the Gravity Recovery and Climate Experiment (GRACE) Satellite Mission: A Review. *Remote Sensing,*

10(6), 829. doi:10.3390/rs10060829

Frappart, F., Ramillien, G., & Ronchail, J. (2013). Changes in terrestrial water storageversusrainfall and discharges in the Amazon basin. *International Journal of Climatology, 33*(14), 3029-3046. doi:10.1002/joc.3647

Gao, C., Lu, Y., & Shi, H. (2019). Detection and analysis of ice sheet mass changes over 27 Antarctic drainage systems from GRACE RL06 data. *Chinese Journal of Geophysics(in Chinese), 62*(3), 864-882. doi:10.6038/cjg2019M0586

Ghiggi, G., Humphrey, V., Seneviratne, S. I., & Gudmundsson, L. (2019). GRUN: An observations-based global gridded runoff dataset from 1902 to 2014. *Earth System Science Data Discussions*, 1-32. doi:10.5194/essd-2019-32

Guo, J., Wang, Z., Bai, B., & Lu, Y. (2006). The analysis of abrupt climate change caused by meteorological stations moving in Yunnan. *Yunnan geographic environment research, 18*(2), 48-52.

Guo, W., Liu, S., Xu, J., Wu, L., Shangguan, D., Yao, X., . . . Liu, Q. (2015). The second Chinese glacier inventory: data, methods and results. *Journal of Glaciology, 61*(226), 357-372.

Han, S. C., Shum, C. K., Jekeli, C., Kuo, C. Y., Wilson, C., & Seo, K. W. (2005). Non-isotropic filtering of GRACE temporal gravity for geophysical signal enhancement. *Geophysical Journal International, 163*(1), 18-25.

Hu, W., Liu, H., Bao, A., & El-Tantawi, A. M. (2018). Influences of environmental changes on water storage variations in Central Asia. *Journal of Geographical Sciences, 28*(7), 985-1000. doi:10.1007/s11442-018-1517-6

Huang, Y., Salama, M. S., Krol, M. S., Su, Z., Hoekstra, A. Y., Zeng, Y., & Zhou, Y. (2015). Estimation of human-induced changes in terrestrial water storage through integration of GRACE satellite detection and hydrological modeling: A case study of the Yangtze River basin. *Water Resources Research, 51*(10), 8494-8516. doi:10.1002/2015wr016923

Huffman, G. J., Bolvin, D. T., Nelkin, E. J., Wolff, D. B., Adler, R. F., Gu, G., . . . Stocker, E. F. (2007). The TRMM Multisatellite Precipitation Analysis (TMPA): Quasi-Global, Multiyear, Combined-Sensor Precipitation Estimates at Fine Scales. *Journal of Hydrometeorology, 8*(1), 38-55. doi:10.1175/jhm560.1

Jacob, T., Wahr, J., Pfeffer, W. T., & Swenson, S. (2012). Recent contributions of glaciers and ice caps to sea level rise. *Nature, 482*(7386), 514-518.

Jia, W., & Xuejie, G. (2013). A gridded daily observation dataset over China region and comparison with the other datasets. *Chinese Journal of Geophysics, 56*(4), 1102-1111.

Junzhi, L., A-Xing, Z., & Zheng, D. (2012). Evaluation of TRMM 3B42 Precipitation Product using Rain Gauge Data in Meichuan Watershed, Poyang Lake Basin, China. *Journal of Resources and Ecology, 3*(4), 359-366. doi:10.5814/j.issn.1674-764x.2012.04.009

Kääb, A., Treichler, D., Nuth, C., & Berthier, E. (2015). Brief Communication: Contending estimates of 2003–2008 glacier mass balance over the Pamir–Karakoram–Himalaya. *The Cryosphere, 9*(2), 557-564. doi:10.5194/tc-9-557-2015

Khaki, M., Forootan, E., Kuhn, M., Awange, J., Dijk, A. I. J. M. V., Schumacher, M., & Sharifi, M. A. (2018). Determining Water Storage Depletion within Iran by Assimilating GRACE data into the W3RA Hydrological Model. *Advances in Water Resources, 114*.

Khandu, Forootan, E., Schumacher, M., Awange, J. L., & Müller Schmied, H. (2016). Exploring the influence of precipitation extremes and human water use on total water storage (TWS)

changes in the Ganges-Brahmaputra-Meghna River Basin. *Water Resources Research, 52*(3), 2240-2258. doi:10.1002/2015wr018113

Klees R , Z. E. A., Winsemius H C , et al. . (2006). The bias in GRACE estimates of continental water storage variations. *Hydrology and Earth System Sciences Discussions, 11*.

Li, T., Wang, B., Chang, C. P., Zhang, Y., & Li, P. T. (2018). A theory for the Indian Ocean dipole mode. *J.atmos.sci, 60*(17), 2119-2135.

LI, W., Wang, W., Zhang, C. Y., Yang, Q., Feng, W., & Liu, Y. (2018). Monitoring groundwater storage variations in the Guanzhong area using GRACE satellite gravity data. *Chinese Journal of Geophysics*.

Li, X., Long, D., Huang, Q., Han, P., Zhao, F., & Wada, Y. (2019). High-temporal-resolution water level and storage change data sets for lakes on the Tibetan Plateau during 2000–2017 using multiple altimetric missions and Landsat-derived lake shoreline positions. *Earth System Science Data, 11*(4), 1603-1627. doi:10.5194/essd-11-1603-2019

Long, D., Scanlon, B. R., Longuevergne, L., Sun, A. Y., Fernando, D. N., & Save, H. (2013). GRACE satellite monitoring of large depletion in water storage in response to the 2011 drought in Texas. *Geophysical Research Letters, 40*(13), 3395-3401. doi:10.1002/grl.50655

Longuevergne, L., Scanlon, B. R., & Wilson, C. R. (2010). GRACE Hydrological estimates for small basins: Evaluating processing approaches on the High Plains Aquifer, USA. *Water Resources Research, 46*(11), 6291-6297.

Luo, Y. (2009). *Research on Geologic Environment in Three Parallel Rivers Region.* China University of Geosciences (Beijing),

Luo, Z., Yao, C., Li, Q., & Huang, Z. (2016). Terrestrial water storage changes over the Pearl River Basin from GRACE and connections with Pacific climate variability. *Geodesy and Geodynamics, 7*(3), 171-179. doi:10.1016/j.geog.2016.04.008

Matthew, R., Isabella, V., & Famiglietti, J. S. (2009). Satellite-based estimates of groundwater depletion in India. *Nature, 460*(7258), 999-1002.

Meng, F., Su, F., Li, Y., & Tong, K. (2019). Changes in Terrestrial Water Storage During 2003–2014 and Possible Causes in Tibetan Plateau. *Journal of Geophysical Research: Atmospheres, 124*(6), 2909-2931. doi:10.1029/2018jd029552

Ni, S., Chen, J., Jin, L., Chao, C., Liang, Q., Observatory, S. A., & CAS. (2014). TERRESTRIAL WATER STORAGE CHANGE IN THE YANGTZE AND YELLOW RIVER BASINS FROM GRACE TIME-VARIABLE GRAVITY MEASUREMENTS. *Journal of Geodesy & Geodynamics*.

Peng, X. (2018). *Spatial-temporal variations of seasonally frozen ground and its response to climate change in the Northern Hemisphere.* (Doctor), Lanzhou University,

Pritchard, H. D. (2017). Asia's glaciers are a regionally important buffer against drought. *Nature, 545*(7653), 169-174. doi:10.1038/nature22062

Qiong, L. I., Luo, Z. C., Zhong, B., & Wang, H. H. (2013). Terrestrial water storage changes of the 2010 southwest China drought detected by GRACE temporal gravity field. *Chinese Journal of Geophysics, 56*(6), 1843-1849.

Rodell, M., Famiglietti, J. S., Wiese, D. N., Reager, J. T., Beaudoing, H. K., Landerer, F. W., & Lo, M. H. (2018). Emerging trends in global freshwater availability. *Nature, 557*(7707), 651-659. doi:10.1038/s41586-018-0123-1

Rodell, M., Houser, P. R., Jambor, U., Gottschalck, J., Mitchell, K., Meng, C. J., . . . Toll, D. (2004).

The Global Land Data Assimilation System. *Bulletin of the American Meteorological Society, 85*(3), 381-394. doi:10.1175/bams-85-3-381

Rojo, J., Rivero, R., Romero-Morte, J., Fernandez-Gonzalez, F., & Perez-Badia, R. (2017). Modeling pollen time series using seasonal-trend decomposition procedure based on LOESS smoothing. *Int J Biometeorol, 61*(2), 335-348. doi:10.1007/s00484-016-1215-y

RONG Yanshu, G. L., LU Shoude. (2018). Analysis on characteristics and causes of persistent meteorological and hydrological drought in Yunnan from 2009 to 2014. *WATER RESOURCES PROTECTION, 34*(3). doi:10. 3880 / j . issn. 1004-6933. 2018. 03. 04

Sanchez-Vazquez, M. J., Nielen, M., Gunn, G. J., & Lewis, F. I. (2012). Using seasonal-trend decomposition based on loess (STL) to explore temporal patterns of pneumonic lesions in finishing pigs slaughtered in England, 2005-2011. *Prev Vet Med, 104*(1-2), 65-73. doi:10.1016/j.prevetmed.2011.11.003

Save, H. (2017). *Status of CSR RL06 GRACE reprocessing and preliminary results.* Paper presented at the Agu Fall Meeting.

Shrestha, M., Koike, T., Hirabayashi, Y., Xue, Y., Wang, L., Rasul, G., & Ahmad, B. (2015). Integrated simulation of snow and glacier melt in water and energy balance-based, distributed hydrological modeling framework at Hunza River Basin of Pakistan Karakoram region. *Journal of Geophysical Research: Atmospheres, 120*(10), 4889-4919. doi:10.1002/2014jd022666

Su, T., & Feng, G. (2015). Spatial-temporal variation characteristics of global evaporation revealed by eight reanalyses. *Science China Earth Sciences, 45*(3), 351-365. doi:10.1007/s11430-014-4947-8

Swenson, S., & Wahr, J. (2006). Post-processing removal of correlated errors in GRACE data. *Geophysical Research Letters, 33*(8). doi:10.1029/2005gl025285

Swenson, S., & Wahr, J. (2007). Multi-sensor analysis of water storage variations of the Caspian Sea. *Geophysical Research Letters, 34*(341), 245-250.

Syed, T. H., Famiglietti, J. S., Rodell, M., Chen, J., & Wilson, C. R. (2008). Analysis of terrestrial water storage changes from GRACE and GLDAS. *Water Resources Research, 44*(2). doi:10.1029/2006wr005779

Tangdamrongsub, N., Hwang, C., & Kao, Y.-C. (2011). Water storage loss in central and south Asia from GRACE satellite gravity: correlations with climate data. *Natural Hazards, 59*(2), 749-769. doi:10.1007/s11069-011-9793-9

Tapley, B. D., Bettadpur, S., Watkins, M., & Reigber, C. (2004). The gravity recovery and climate experiment: Mission overview and early results. *Geophysical Research Letters, 31*(9), 4 PP.

Wahr, J., Molenaar, M., & Bryan, F. (1998). Time variability of the Earth's gravity field: Hydrological and oceanic effects and their possible detection using GRACE. *Journal of Geophysical Research: Solid Earth, 103*(B12), 30205-30229. doi:10.1029/98jb02844

Wang, B., & Fan, Z. Choice of South Asian Summer Monsoon Indices. *Bull.amer.meteor.soc, 80*(4), 629-638.

Wang, J., Jiang, D., Huang, Y., & Wang, H. (2014). Drought analysis of the Haihe river basin based on GRACE terrestrial water storage. *ScientificWorldJournal, 2014*, 578372. doi:10.1155/2014/578372

Wang, L., Kaban, M., Thomas, M., Chen, C., & Ma, X. (2019). The Challenge of Spatial Resolutions for GRACE-Based Estimates Volume Changes of Larger Man-Made Lake: The Case of

China's Three Gorges Reservoir in the Yangtze River. *Remote Sensing, 11*(1), 99. doi:10.3390/rs11010099

Wanqin, G. U. O., Junli, X. U., Shiyin, L. I. U., Donghui, S., Lizong, W. U., Xiaojun, Y. A. O., . . . Yuan, W. (2014). The Second Glacier Inventory Dataset of China (Version 1.0). *Cold and Arid Regions Science Data Center at Lanzhou*. doi:10.3972/glacier.001.2013.db

doi:10.3972/glacier.001.2013.db

Wu, Q., Si, B., He, H., & Wu, P. (2019). Determining Regional-Scale Groundwater Recharge with GRACE and GLDAS. *Remote Sensing, 11*(2), 154. doi:10.3390/rs11020154

Xia, L., Gao, Y., Wang, W., Lan, Y., Xu, J., & Kai, L. (2014). Climate Change and Applicability of GLDAS in the Headwater of the Yellow River Basin. *Advances in Earth Science, 29*(4), 531-540.

Yang, D., Yang, H., & Lei, H. (2014). *Watershed Hydrology*. Beijing: TSINGHUA University Press.

Yang, P., Xia, J., Zhan, C., Qiao, Y., & Wang, Y. (2017). Monitoring the spatio-temporal changes of terrestrial water storage using GRACE data in the Tarim River basin between 2002 and 2015. *Science of The Total Environment, 595*, 218-228. doi:10.1016/j.scitotenv.2017.03.268

Yang, P., Xia, J., Zhan, C., & Wang, T. (2018). Reconstruction of terrestrial water storage anomalies in Northwest China during 1948–2002 using GRACE and GLDAS products. *Hydrology Research*, nh2018074. doi:10.2166/nh.2018.074

Yang, T., Wang, C., Chen, Y., Chen, X., & Yu, Z. (2015). Climate change and water storage variability over an arid endorheic region. *Journal of Hydrology, 529*, 330-339. doi:10.1016/j.jhydrol.2015.07.051

Yang, W., Yao, T., Xu, B., Ma, L., Wang, Z., & Wan, M. (2010). Characteristics of recent temperat glacier fluctuations in the Parlang Zangbo River basin, soutbeast Tibetan Pla-teau. *Chinese Sci Bull, 55*(18), 1775-1780. doi:10.1007/s11434-010-3214-4

Yao, T., Shilong, P., Shen, M., Jing, G., Wei, Y., Zhang, G., . . . Xu, B. (2017). Chained Impacts on Modern Environment of Interaction between Westerlies and Indian Monsoon on Tibetan Plateau. *Bulletin of Chinese Academy of Sciences*.

Zhang, L., Wang, J., Huang, Y., Hao, W. U., & Duan, Q. C. (2015). Characteristics of drought based on standardized precipitation evapotranspiration index from 1961 to 2010 in Yunnan province. *Journal of Meteorology & Environment*.

Zhang, W., Yi, Y., Jafarov, E. E., Yang, K., Kimball, J. S., & Song, K. (2015). *Simulation of Permafrost and Seasonally Frozen Ground Conditions and their Response to Recent Climate Warming in the Tibetan Plateau.* Paper presented at the Agu Fall Meeting.

Zhao, K., & Li, X. (2017). Estimating terrestrial water storage changes in the Tarim River Basin using GRACE data. *Geophysical Journal International, 211*(3), 1449-1460. doi:10.1093/gji/ggx378

Zhao, Q., Ding, Y., Wang, J., Gao, H., Zhang, S., Zhao, C., . . . Shangguan, D. (2019). Projecting climate change impacts on hydrological processes on the Tibetan Plateau with model calibration against the glacier inventory data and observed streamflow. *Journal of Hydrology, 573*, 60-81. doi:10.1016/j.jhydrol.2019.03.043

Zhen, L., Chuanyin, Z., Baogui, K., Yang, L., Wanqiu, L., & Cai, Y. (2018). North China Plain Water Storage Variation Analysis Based on GRACE and Seasonal Influence Considering. *Acta Geodaetica Et Cartographica Sinica*.

Zhong, Y., Zhong, M., Feng, W., Zhang, Z., Shen, Y., & Wu, D. (2018). Groundwater Depletion in the West Liaohe River Basin, China and Its Implications Revealed by GRACE and In Situ

Measurements. *Remote Sensing, 10*(4), 493. doi:10.3390/rs10040493

Zhou, Y., Li, Z., Li, J., Zhao, R., & Ding, X. (2018). Glacier mass balance in the Qinghai–Tibet Plateau and its surroundings from the mid-1970s to 2000 based on Hexagon KH-9 and SRTM DEMs. *Remote Sensing of Environment, 210*, 96-112. doi:10.1016/j.rse.2018.03.020